Received: 29 September 2023 | Revised: 1 November 2023 | Accepted: 10 November 2023

DOI: 10.1002/eom2.12426

RESEARCH ARTICLE

EcoMat FUNCTIONAL MATERIALS FOR GREEN ENERGY AND ENVIRONMENT WILEY

Concave microlens arrays with tunable curvature for enhanced photodegradation of organic pollutants in water: A non-contact approach

Qiuyun Lu[1] | **Yanan Li**[1] | **Kehinde Kassim**[1] | **Ben Bin Xu**[2] | **Mohamed Gamal El-Din**[3] | **Xuehua Zhang**[1]

[1]Department of Chemical and Materials Engineering, University of Alberta, Edmonton, Alberta, Canada

[2]Smart Materials and Surfaces Lab, Mechanical and Construction Engineering, Faculty of Engineering and Environment, Northumbria University, Newcastle upon Tyne, UK

[3]Department of Civil and Environmental Engineering, University of Alberta, Edmonton, Alberta, Canada

Correspondence

Mohamed Gamal El-Din and Xuehua Zhang, Department of Civil and Environmental Engineering, University of Alberta, Edmonton, T6G 1H9 Alberta, Canada.
Email: mgamalel-din@ualberta.ca and xuehua.zhang@ualberta.ca

Ben Bin Xu, Smart Materials and Surfaces Lab, Mechanical and Construction Engineering, Faculty of Engineering and Environment, Northumbria University, Newcastle upon Tyne, NE1 8ST, UK.
Email: ben.xu@northumbria.ac.uk

Funding information

Canada First Research Excellence Fund; Canada Foundation for Innovation; Canada Research Chairs; Natural Sciences and Engineering Research Council of Canada; NSERC Alliance - Alberta Innovates (AI) Advance grants;

Abstract

Solar-driven photodegradation for water treatment faces challenges such as low energy conversion rates, high maintenance costs, and over-sensitivity to the environment. In this study, we develop reusable concave microlens arrays (MLAs) for more efficient solar photodegradation by optimizing light distribution. Concave MLAs with the base radius of ~5 μm are fabricated by imprinting convex MLAs to polydimethylsiloxane elastomers. Concave MLAs possess a non-contact reactor configuration, preventing MLAs from detaching or being contaminated. By precisely controlling the solvent exchange, concave MLAs are fabricated with well-defined curvature and adjustable volume on femtoliter scale. The focusing effects of MLAs are examined, and good agreement is presented between experiments and simulations. The photodegradation efficiency of organic pollutants in water is significantly enhanced by 5.1-fold, attributed to higher intensity at focal points of concave MLAs. Furthermore, enhanced photodegradation by concave MLAs is demonstrated under low light irradiation, applicable to real river water and highly turbid water.

KEYWORDS

microlens array, photodegradation, solar energy, water treatment

Abbreviations: 3D, three-dimensional; AFM, atomic force microscope; CBZ, carbendazim; CVD, chemical vapor deposition; HDODA, 1,6-hexanediol diacrylate; LMA, lauryl methacrylate; ML(s), microlens(es); MLA(s), microlens array(s); MO, methyl orange; PDMS, polydimethylsiloxane; PFOTS, perfluorodecyltrichlorosilane; PHDODA, poly(1,6-hexanedioldiacrylate); PLMA, poly(lauryl methacrylate); SEM, scanning electron microscope; TOC, total organic carbon; UV–vis, ultraviolet–visible.

Engineering and Physical Sciences Research Council (EPSRC, UK), Grant/Award Number: RiR grant - RIR18221018-1

1 | INTRODUCTION

Solar-driven photodegradation represents a sustainable and environment-friendly process to harness solar energy to remove organic pollutants in water. For example, solar disinfection has been used by around 4.5 billion people around the world for water decontamination.[1] Several challenges of solar-driven photodegradation have been identified as the restricted conversion rate of solar energy to chemical energy,[2] scaling up the reactor,[3] and the decentralized and intermittent features of solar irradiation.[4,5] Microlenses (MLs) have emerged as a promising technology to enhance energy transfer efficiency by optimizing light inside of the solar-driven reactors.[6–9] The near-field effect of MLs enables the strong focusing effects in a short distance around the MLs,[10,11] which has been widely applied in the fields where high light harvesting efficiency[12–17] and minimized dimensions[18–20] are required. The focal distance of typical convex MLs is in the scale of micrometers,[11,21,22] so they have to be implemented inside of a reactor to make focal points located inside water.[23,24] While this in-contact configuration may accelerate the deterioration of MLs, the introduction of secondary contamination to the treated water seems inevitable with the aging of microlens arrays (MLAs).[25] By far, MLs arranged in a non-contact configuration as a potential alternative choice remain to be explored.

The function of MLs in an optical system is to regulate light, subject to their geometrical features and spatial arrangement. When MLs are arranged in specific patterns, that is, MLAs, they can generate stronger focusing effects within finite space compared with the MLs that are randomly distributed on substrates.[23] Concave MLAs, which are embedded into matrices, have the potential to be integrated into solar-water reactors in a non-contact configuration. Current fabrication technologies of concave MLAs can be classified into direct and indirect methods. In direct fabrication methods, no templates are required, and concave MLAs are directly obtained. For example, mechanical machining,[26–28] thermal manipulating,[29,30] or direct laser writing[31–33] helps to create indentations that function as MLAs on the surface of matrices. Chemical wet-etching is another method to directly form concave MLAs, where materials on the unprotected regions can be selectively removed after being immersed into etchants.[34–36] The requirements for precision and the expenses are too high in mechanical machining or laser writing, while the wet-etching method can hardly prepare concave MLAs with the desired shape.

In indirect fabrication methods, concave MLAs are imprinted from templates, and the shape and spatial arrangement of concave MLAs are dependent on that of the masterpieces.[37–39] Breath-figure is one of the methods where the condensed water droplets can be used as templates to produce the concave MLAs.[37,38] However, the uniformity of concave MLAs is hard to control during the condensation process.[39] In another typical indirect method, soft lithography, multiple concave MLAs can be fabricated from the same mother template, and the high transparency of commonly used silane for the method makes it widely applied in optoelectronic devices.[40–43]

In soft lithography, convex MLAs usually act as mother templates to prepare concave MLAs. To precisely control the shape and uniformity of convex MLAs as templates, several technologies have been developed,[19] such as hot embossing,[44,45] thermal reflowing,[46,47] inkjet printing technology,[29,48,49] and laser-based fabrication methods.[42,50] Among all reported methods, there is one type that convex MLAs can be made by locally photopolymerizing surface microdroplets obtained from a solvent exchange process, which is highly desired to produce mother templates for concave MLAs.[51,52] In this solvent exchange approach, surface microdroplets containing monomers and photoinitiators form on pre-patterned substrates due to oversaturation.[53] By modifying monomer concentration gradients,[54] flow conditions,[53,55] and substrate wettability,[56] microdroplet growth is effectively controlled, enabling precise tuning of the dimension and curvature of convex MLAs.[57,58] Even though convex MLAs made by the solvent-based method show flexibility in fabrication, the risk of damage is unpreventable for the convex MLAs when they are immersed in aqueous phase to get desired enhancement in photodegradation. It is more promising to use such convex MLAs as templates to develop non-contact concave MLAs for solar reactors with enhanced decontamination efficiency, which has not been reported yet.

In this work, we design and fabricate non-contact concave MLAs with tunable curvatures by repeatably imprinting polymeric convex MLAs. Convex MLAs work as templates are generated by solvent exchange followed by local photopolymerization. The focusing effects of concave MLAs are evidenced by optical simulations and experimental observation under confocal microscopy. Through the light treatment under simulated solar light, the performance of concave MLAs with varying aspect ratios in photodegradation is examined upon suppressed irradiation in real river water and

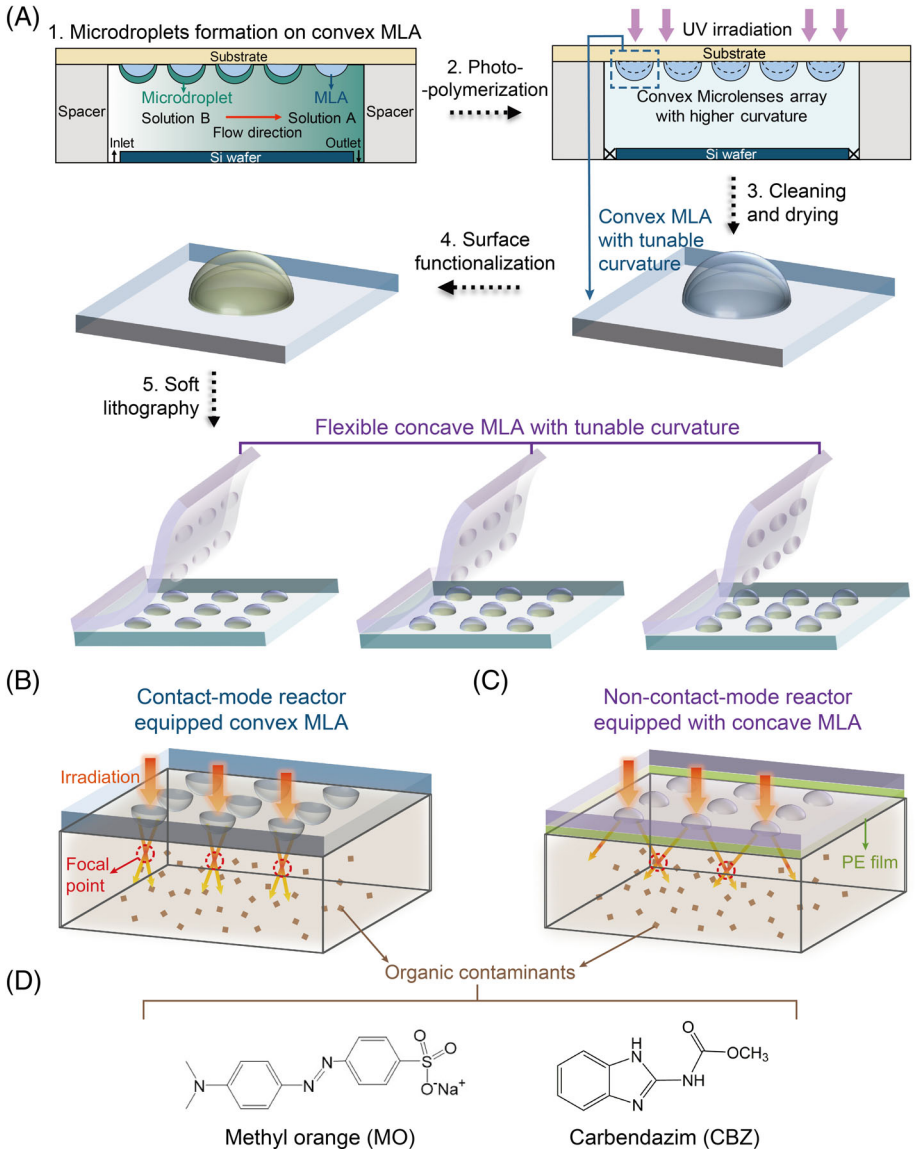

FIGURE 1 (A) The fabrication process of convex and concave microlens arrays (MLAs) with tunable curvatures. The sketch of the self-assembled (B) contact-mode reactor integrated with convex MLAs and (C) non-contact-mode reactor integrated with concave MLAs, concave MLAs were separated from the aqueous phase by a transparent PE film (thickness: ~12 μm). The length, width, and thickness of the reactors in (B) and (C) is 90, 80, and 1 mm, respectively. (D) Chemical structures of the organic pollutants used in the photodegradation, including methyl orange (MO) and carbendazim (CBZ).

synthetic high-turbidity water. Concave MLAs are integrated into solar-driven reactors in a non-contact configuration further providing a sustainable approach to enhance photodegradation in complicated water matrices while mitigating the risks of MLAs damage and secondary contamination.

2 | RESULTS AND DISCUSSION

The fabrication process of concave MLAs with tunable curvatures and the concept of concave MLAs-coupled solar water reactors are displayed in (Figure 1). First, convex MLAs as templates are prepared through the solvent exchange process, where prepatterned substrates or convex MLAs themselves can be used as substrates (Figure 1A). Surface microdroplets prefer to form on hydrophobic domains or on top of microlenses due to the lower surface energy than on the surrounding area.[57] After the UV curing step (Figure 1A), surface microdroplets are cured into the polymer MLAs, and the microdroplet-on-microlens structures transform into new MLAs with higher curvature. Through soft lithography (Figure 1A3–5), multiple concave MLAs made of polydimethylsiloxane (PDMS) elastomers are obtained from the same templates. By adjusting the fabrication conditions of templates, the tunability of concave MLAs curvature is achieved. Both convex MLAs and concave MLAs are integrated into self-assembled solar water reactors, in a contact and a non-contact configuration, respectively (Figure 1B). Photodegradation of methyl orange (MO) and carbendazim (CBZ) is conducted under simulated solar to investigate the effectiveness of MLAs in enhancing reaction efficiency.

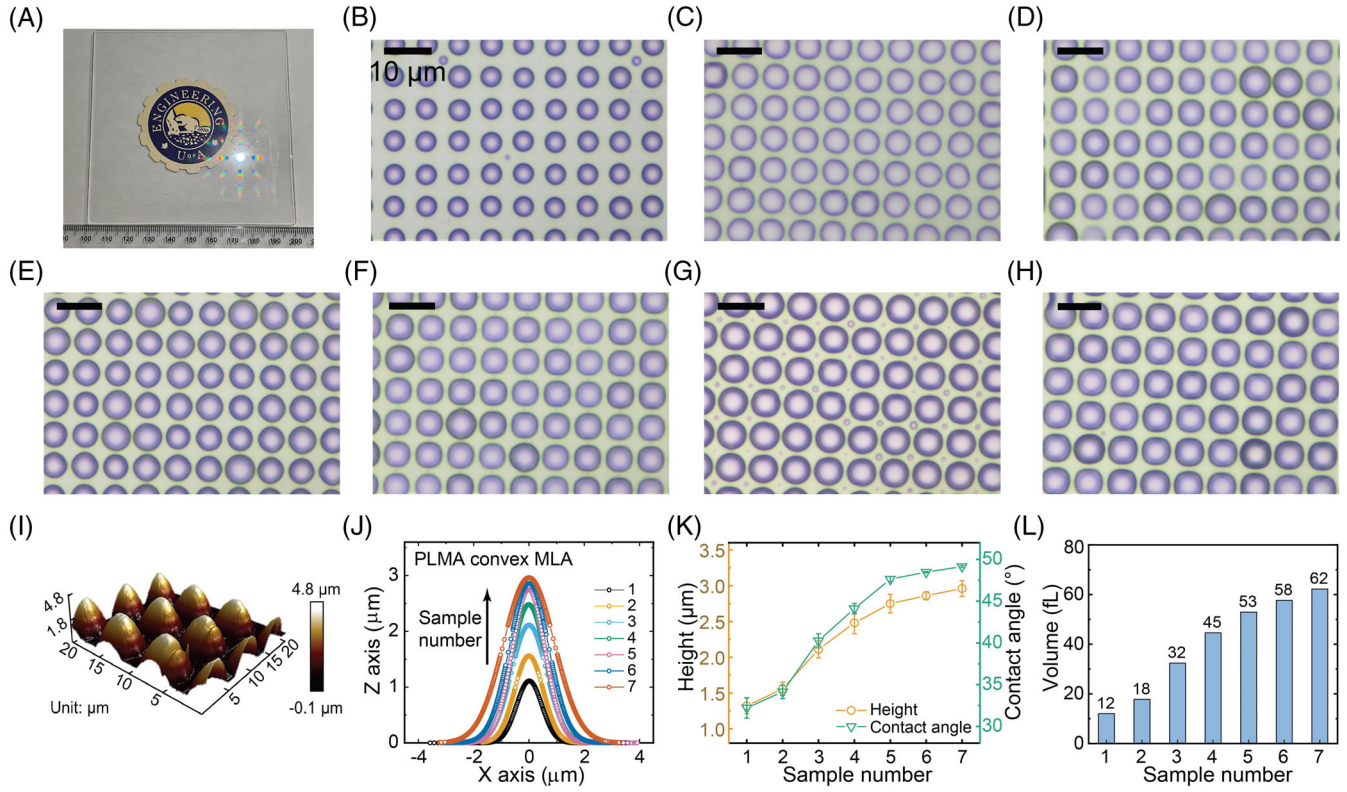

FIGURE 2 (A) A photo of a convex microlens array (MLA) (sample 10) on a 4-inch square glass substrate, and the photo is taken by a phone camera with a flashlight. Photos of the poly(lauryl methacrylate) (PLMA) MLA from (B) sample 1, (C) sample 2, (D) sample 3, (E) sample 4, (F) sample 5, (G) sample 6, and (H) sample 7 caught by optical microscope (Table 2). (I) The 3D profile of a representative PLMA MLA from an AFM. (J) Cross-sectional profiles of single MLs from each PLMA convex MLA sample, obtained by a confocal microscope. (K) Height and contact angle of a single ML in each PLMA convex MLA sample (L) The volume of a single ML in each PLMA convex MLA sample (Unit: femtoliter, i.e., fL).

2.1 | Geometric morphology and optical properties of convex MLAs

Convex MLAs immobilized on glass slides with areas presented good transparency. The array of colorful light spots in Figure 2A indicates the highly ordered structures within an area as large as 100 cm^2. In order to track the change of the curvature of convex MLAs, the PLMA convex MLAs on sample 1–7 (Table 2) are analyzed and compared as follow. The top view of each PLMA convex is presented in the photos captured through an optical microscope (Figure 2B–H). A representative 3D profile of MLA obtained by AFM is shown in Figure 2I. The cross-sectional profiles of single MLs from seven samples are extracted from the 3D graph and are displayed by the Z-X plot in Figure 2J. With the analysis with ImageJ, the lateral radius and surface coverage rate of sample 1–7 are measured (Figure S1). The lateral radius (r) of a convex ML in the array increases between 2.3 and 3.2 μm from sample 1 to sample 7, resulting in the surface coverage rate varying between 31% and 64%. According to the Z-X plot from AFM, the MLA with a larger sample number is higher, and the pitch height (h) reaches around 3 μm in sample 7. The contact angles of convex MLAs in different samples are calculated by assuming the MLs in spherical shape in Figure 2K, which can be tuned from 32° to 49°.

Based on the lateral size and height of PLMA convex MLAs, the volume of a single ML in each convex MLA is obtained and summarized in Figure 2L. With our method, the volume of each ML can be controlled on a femtoliter scale, which involves only 10^{-14} M monomers in the photopolymerization process. The precise control of the volume of each ML is attributed to the well-controlled diffusive growth of the microdroplets during the solvent exchange. The diffusive growth process is driven by the concentration gradient of the monomer at the wavefront and affected by the flow rate during the solvent exchange. Either a higher concentration of monomer in solution A or the larger flow rate of solvent exchange speeds up the diffusive growth of the microdroplets. Surface microdroplets selectively form within hydrophobic domains on the pre-patterned substrate or on top of previous convex MLA due to the lower surface tension at those spots. As a result, the microdroplets with higher diffusive growth rates present slight lateral expansions but an obvious enhancement of height. PHDODA

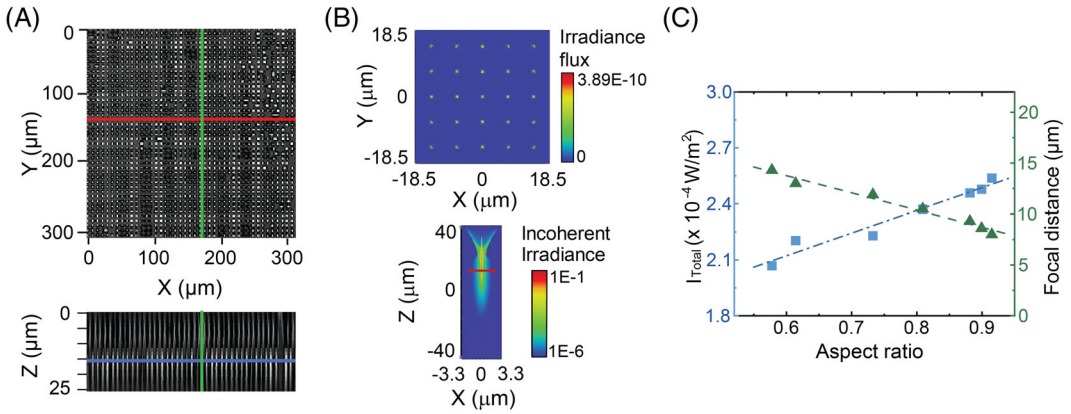

FIGURE 3 (A) Top view at focal points (up) and cross-sectional view (down) light intensity profiles of sample 1 captured by the confocal microscope. (B) Top view at focal points (up) and cross-sectional view (down) light intensity profiles of sample 1 obtained by optical simulations. (C) The trend of the total intensity at the focal points of MLs within an area of 1 cm^2 (I_{Total}) or focal distance over the aspect ratio (h/r) of each PLMA convex MLA. ML, microlens; MLA, microlens array; PLMA, poly(lauryl methacrylate).

convex MLAs with tunable curvature are successful with the same procedure as well, suggesting the universality of the fabricating method.

The focusing effect of MLAs is revealed via confocal microscopy and optical simulations. As illustrated in Figure 1B, the light rays passing through a convex MLA are expected to converge, generating a focal point with stronger light intensity. The confocal microscope experimentally captures the actual 3D light intensity profiles of MLAs (Figure S3). The representative top view and cross-sectional view intensity profiles extracted from 3D intensity profiles in sample 1 are displayed in (Figure 3A). The top view intensity profile shows that the brightest light spots are arranged in arrays, in agreement with the focusing effects predicted in the possible light paths in Figure 1B. According to the cross-sectional intensity profiles, the focal distance of each convex MLA is measured, which decreases from 16 μm in sample 1 to 7 μm in sample 7.

The top view and cross-sectional view intensity profiles of convex MLAs can also be built through optical simulations (Figure S2). For instance, the intensity profiles of sample 1 by simulations are illustrated in Figure 3B. The focal distances of MLAs obtained by optical simulations change between 14 and 8 μm, which are close to the results measured by confocal microscopy. Apart from validating the experimental results by confocal microscopy, the light intensity value at the focal points of each convex MLA can be calculated by optical simulations. The highest peak intensity value is observed in sample 7, which is around 5.17×10^{-10} W/m^2, 33% higher than that in sample 1.

The correlation of I_{Total} and the focal distance of a convex MLA with the aspect ratio (h/r) of the MLA is suggested in Figure 3C. As the aspect ratio of the MLA gets larger from 0.57 to 0.92, I_{Total} linearly decreases with the focal distance linearly decreases. The correlation provides guidance for the fine-tuning of MLA curvature by the solvent exchange process to achieve the desired focusing effect level.

2.2 | Geometric morphology and optical properties of concave MLAs

After the soft lithography process, the concave MLAs are obtained on the surface of flexible PDMS films with a thickness of around 1 mm. The appearance of the PDMS film with a concave is displayed in Figure 4A, indicating the flexibility of the concave MLA embedded film. The transmittance of all concave MLA samples utilized in photodegradation experiments is over 90% under the light with the wavelength from 300 to 1000 nm (Figure S6) The photos captured by the optical microscope of the concave MLAs and corresponding convex MLAs templates are presented in Figure 4B,C). A sketch of the cross-sectional view of a single concave ML in an array is demonstrated in the sketch in Figure 4D, where r is the lateral radius, d is the depth, and θ is the reverse contact angle of the ML. The concave MLA structure is validated by the scanning electron microscope (SEM) images of the top and cross-sectional surface of the PDMS film in Figure 4E.

According to the optical and SEM images of the concave MLAs, the lateral radius (r) and depth (d) of concave MLAs are obtained and listed in Table 1. The lateral radius of the concave MLAs prepared from PLMA convex MLAs is smaller than the original value in the template due to the possible deformation of PLMA during the PDMS curing step.[59] In comparison, the concave MLAs prepared by using PHDODA convex MLAs as templates

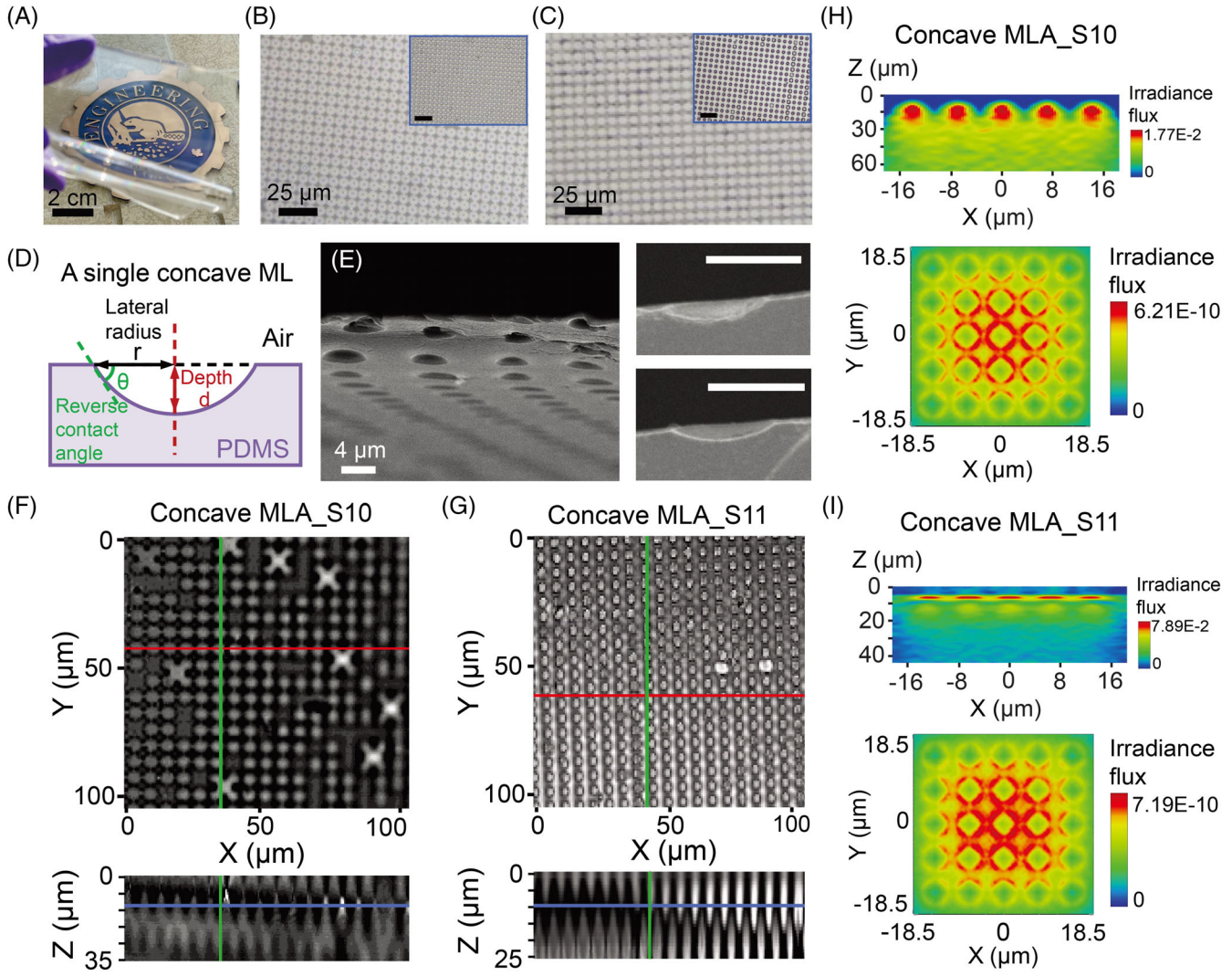

FIGURE 4 (A) A photo of a PDMS film with a concave MLA copied from sample 10 (concave MLA_S10) under natural light. Photos captured by the microscope of concave MLAs on PDMS film (thickness: 1 mm), including (B) the concave MLA using sample 10 as a template (concave MLA_S10) and (C) the concave MLA using sample 11 as a template (concave MLA_S11), and the photo of the corresponding convex MLA template is attached in the right-up corner. (D) A sketch of a single concave ML on PDMS film, r is the lateral radius, d is the depth, and θ is the reverse contact angle of the ML. (E) Photos of concave MLA_S10 in top view and cross-sectional view by SEM (scale bar: 4 μm). Top view (up) and cross-sectional view (down) of light intensity profiles obtained by confocal microscope of (F) concave MLA_S10, and (G) concave MLA_S11 at the horizontal plane where the maximum irradiance flux values are observed. Cross-sectional view intensity profile (up) of a 5×1 MLA and top view intensity profile (down) of a 5×5 MLA from (H) concave MLA_S10, and (I) concave MLA_S11 by optical simulations. MLA, microlens array; PLMA, poly(lauryl methacrylate).

remain the almost same shape and lateral size. Better thermal stability of PHDODA enables the corresponding concave MLAs to remain the same size and shape. To verify the stability of PHDODA convex MLAs during the preparation of concave MLA structures, the microscope images of PHDODA convex MLAs after 1–4 rounds of structure replication are presented in Figure S4. PHDODA convex MLAs remain on the substrate without any deformation after multiple rounds of soft lithography, suggesting the preparation of the concave MLAs on PDMS films is repeatable. Therefore, concave MLAs using PHDODA convex MLAs as templates are mainly discussed below due to the repeatable geometric features.

The redistribution of light passing through concave MLAs can be also illustrated by the intensity profiles obtained by confocal microscopy. As shown in Figure 4F,G, the top view intensity profiles displayed the arrays of brightest spots below the concave MLAs. The Z position of the top view intensity profile is indicated by the blue horizontal line in the corresponding cross-sectional intensity profile below. The brightness of light increase and then decrease as the distance from concave MLAs along the Z axis increases, validating the focusing effects in concave MLAs. For convenience, the spot with the strongest intensity below a concave ML is defined as the focal point of the ML, and the vertical distance

between the focal point and the bottom line of PDMS film is the focal distance. From the intensity profiles by confocal microscopy, the focal points of concave MLAs are found not located at the same planar surface, which is attributed to the deformation of the flexible PDMS film during the characterization. Therefore, average focal distances of concave MLA_S10 and concave MLA_S11 are estimated by analyzing the focal point of each ML included in the 3D intensity profiles, which are around 17 and 9 μm, respectively. However, an essential restriction of the confocal microscope is the difficulty in intensity quantification due to the fluctuated light gaining during the operation, especially for concave MLAs on flexible substrates.

Compared with confocal microscopy, optical simulations can not only track the light paths passing through concave MLAs but also quantify the intensity at certain spots. The simulation results indicate that light diverges and then interferes with each other, creating hot spots in the space close to the concave MLA, which is interpreted in the sketch in Figure 1C and validated by the cross-sectional light intensity profiles obtained from optical simulations (Figure 4H,I). Aside from the cross-sectional intensity profiles, the variation of light intensity can also be reflected by the change of irradiance flux across the top view intensity profiles with depths. For example, the peak light intensity under concave MLA_S10 increases when the depth increases from 0 to 15 μm and then rapidly decreases (Figure 4H). The distances between the spots with the highest intensity values and the substrate bottom in optical simulations are consistent with the results from confocal microscopy.

To compare the strength of focusing effects of all the concave MLAs, the top view of the light intensity profiles with the maximum index flux of concave MLAs is captured for analysis. The strongest peak intensity at the depth of ~15 μm under concave MLA S_10 is nearly 10 times higher than the situation without concave MLAs. Meanwhile, the intensity across the detected horizontal concave MLA S_10 is continuously higher than that under the planar PDMS film from the depth of 15–45 μm. According to Figure 4H,I and Table 1, the concave MLA (concave MLA_S11) made from the convex MLA with larger curvature (sample 11) has a higher peak irradiation flux, which is around 16% higher than that in concave MLA_S10. Compared with the highest peak intensity achieved by convex MLA (sample 7), the peak intensity in concave MLAs is comparable, proving the potential of concave MLAs in enhancing the degradation of organic contaminants.

TABLE 1 Geometric parameters of concave MLAs on PDMS films.

Sample	r (μm)	d (μm)	θ (°)
8	2.29	1.32	58
9	2.54	1.59	64
10	2.63	1.31	53
11	2.78	1.45	55

Abbreviations: MLA, microlens array; PDMS, polydimethylsiloxane.

2.3 | Photodegradation efficiency of an organic contaminant with convex MLAs

Photodegradation efficiency (η) of MO in an aqueous solution with convex MLAs is obviously enhanced, especially with the MLs with higher curvature. The absorbance spectra of MO solution that is irradiated with different convex PLMA MLAs under 1-h irradiation of visible LED light are shown in Figure 5A. With the peak

TABLE 2 Conditions of solvent exchange process in the preparation of convex microlens arrays.

Sample	Substrate	Monomer in solution A	Flow rate (mL/h)
1	Pre-patterned glass (672 mm^2)	2.0 vol% LMA	8
2	Sample 1	1.0 vol% LMA	6
3	Sample 1	2.0 vol% LMA	6
4	Sample 1	3.0 vol% LMA	4
5	Sample 1	4.0 vol% LMA	3
6	Sample 1	4.0 vol% LMA	4
7	Sample 6	2.0 vol% LMA	4
8	Pre-patterned glass (100 cm^2)	2.0 vol% LMA	45
9	Sample 8	2.0 vol% LMA	35
10	Pre-patterned glass (100 cm^2)	3.8 vol% HDODA	35
11	Sample 10	2.0 vol% HDODA	30

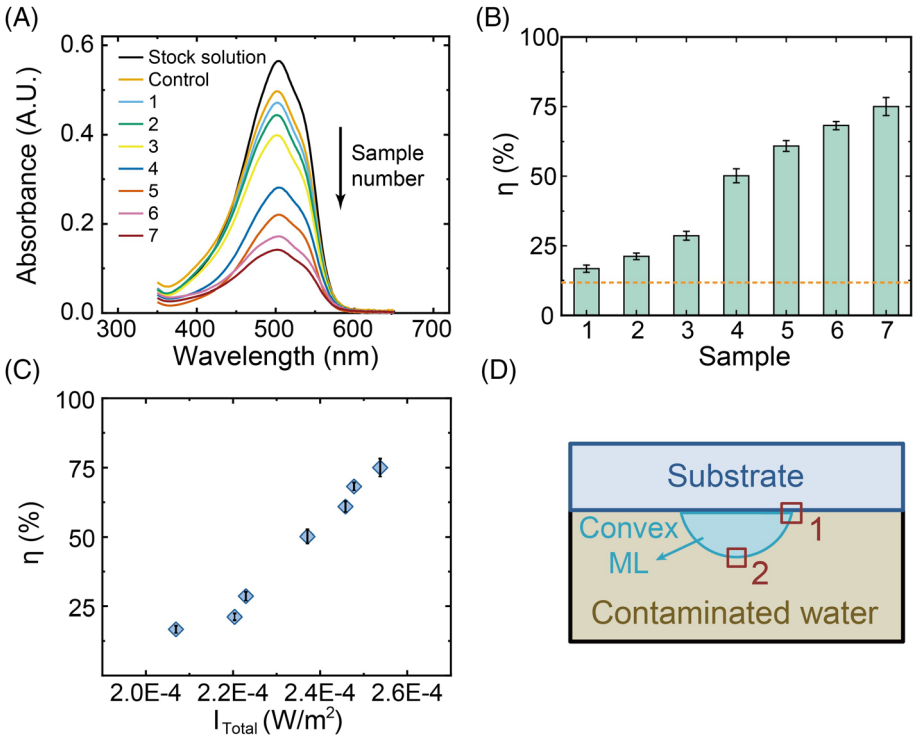

FIGURE 5 (A) Representative absorbance spectra of MO solution (5 mg/L, pH = 3.0) before and after 1-h irradiation of visible LED light (intensity: 21.64 W/cm^2) with PLMA convex MLAs with different curvatures (from sample 1 to 7). (B) Photodegradation efficiency (η) of MO in the reactor equipped with different PLMA convex MLAs, and the dashed line indicates the efficiency in the control group. (C) The correlation between η of MO and I_{Total} of each MLA. (D) A sketch of a cross-sectional view of the contact-mode reactor integrated with convex MLAs, and two spots with the risk of damage are labeled by red squares. MLA, microlens array; MO, methyl orange; PLMA, poly(lauryl methacrylate).

absorbance values, η of MO after the irradiation of 1 h is calculated with Equation (1) and plotted in Figure 5B. All groups with PLMA convex MLAs achieve higher (η) than the control group. From sample 1 to 7, the (η) continuously increases, reaching the maximum value of 75% when sample 7 is applied.

Such enhancement in η is possibly correlated with the stronger focusing effect of MLs with larger curvature. To verify the correlation, I_{Total} is in each convex MLA among sample 1–7, which is the total intensity at the focal points of MLs in the array with an area of 1 cm^2, is defined to quantify the focusing effect of each convex MLAs. As shown in Figure 3C, the convex MLA with a larger curvature has a larger I_{Total}, indicating a stronger focusing effect. In Figure 5C, η of MO is correlated with I_{Total} of convex MLAs, and a positive relationship is presented between the two parameters. Such correlation may assist the design of MLAs for photodegradation reactors with enhanced η. However, the enhancement in η can hardly increase due to the upper limit of the curvature of PLMA convex MLAs in the current method as shown in Figure S5.

Even though a high enhancement in η of MO has been achieved by integrating concave MLAs with higher curvature in the reactor for photodegradation, some risks still exist due to the current contact-mode setup. At the interface of convex MLAs and the glass substrate (Spot 1 in Figure 5D), the risk of water penetration exists since MLAs are fully immersed in the aqueous phase, accelerating the detachment of convex MLA. Another risk is located at the interface of MLAs and the aqueous phase (Spot 2 in Figure 5D). The free radicals produced during the photodegradation mainly existed in the aqueous phase, possibly promoting the degradation of polymeric convex MLAs and posing secondary contamination to the treated water. Consequently, an alternative reactor design to avoid the potential side effects of MLAs without sacrificing the advantages of focusing effects is required.

2.4 | Photodegradation efficiency of organic contaminants with concave MLAs in different water matrices

Concave MLAs have the unique advantage that the whole structure is embedded in a PDMS film, so they would not be physically damaged and can be separated from contaminated water matrices. Additionally, the flexibility of PDMS films enables concave MLAs to be easily bent and wrapped around reactors with various shapes. Based on the above-mentioned features of concave MLAs and their focusing effects, a non-contact mode reactor integrated with concave MLAs is designed for the degradation process (Figure 6A).

The performance of the concave MLAs on PDMS films is investigated in the degradation of MO in different water matrices (Figure 6B,C) under the simulated solar light. For the photodegradation of MO in ultrapure water under simulated solar light at 1 Sun or 0.4 Sun, η in reactors with concave MLAs made from sample 10 to

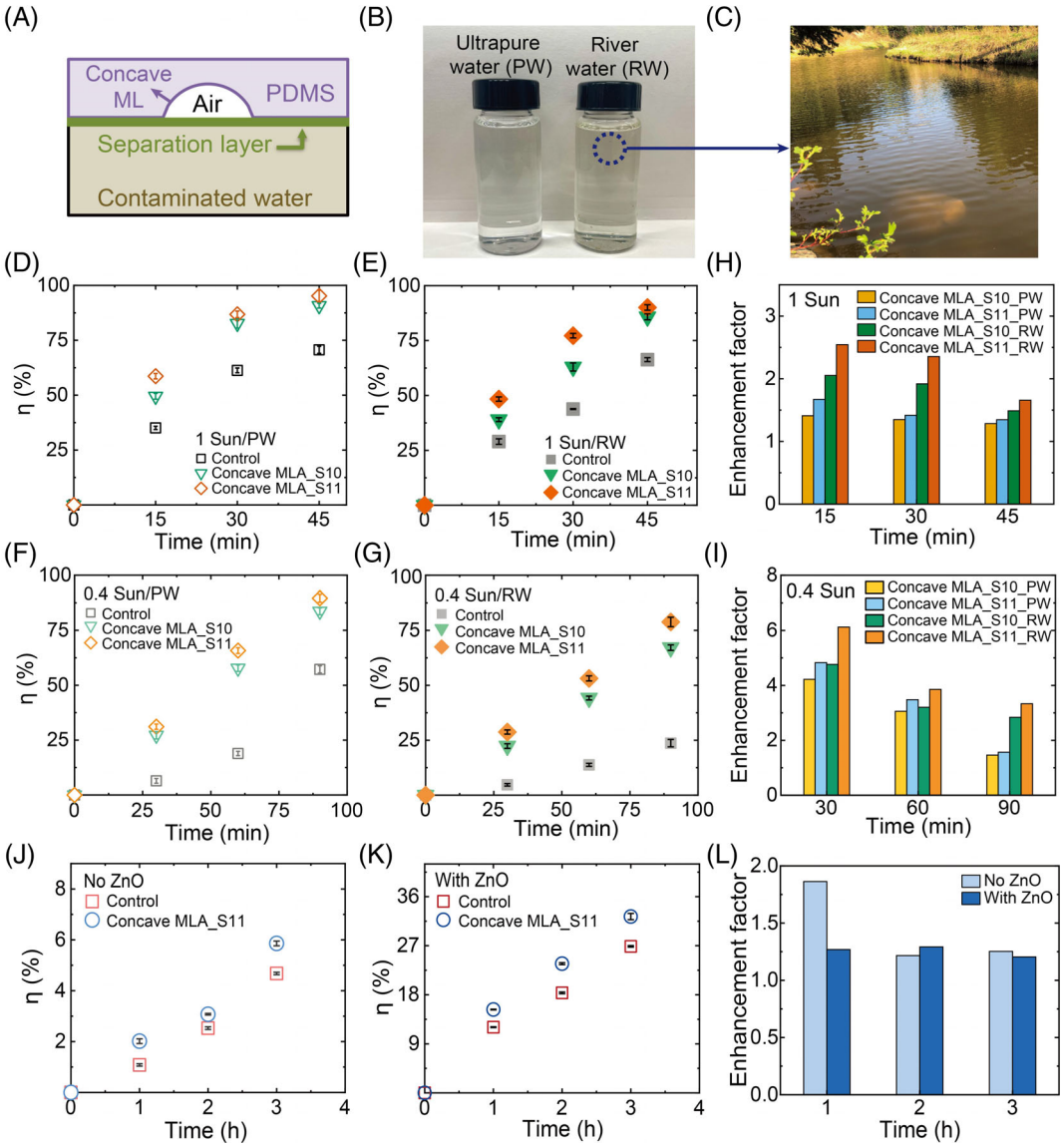

FIGURE 6 (A) A sketch of a cross-sectional view of the non-contact-mode reactor integrated with concave MLAs. (B) A photo of ultrapure water (PW) and river water (RW) used in the preparation of MO solution for light treatment. (C) A photo of the spot for river water collection. The photodegradation efficiency (η) of MO (D) in ultrapure water under simulated solar at 1 Sun, (E) in real river water under simulated solar at 1 Sun, (F) in ultrapure water under simulated solar at 0.4 Sun, (G) in real river water under simulated solar at 0.4 Sun. Enhancement factors of MO photodegradation in different water matrices and with varied concave MLAs under the irradiation of (H) 1 Sun or (I) 0.4 Sun. Photodegradation efficiency (η) of CBZ in ultrapure water (J) without or (K) with ZnO as photocatalyst after the irradiation of simulated solar light (intensity: 1 Sun). (L) Enhancement factors of CBZ photodegradation achieved by the concave MLA made from sample 11 (concave MLA_11) without and with ZnO in the light treatment. ML, microlens; MLA, microlens array; MO, methyl orange.

11 (Table 2) is higher than the control group (Figure 6D,F). When decreasing the light intensity of irradiation, η of MO after the light treatment is lower no matter whether concave MLAs are applied or not. To reach a similar level of degradation, the irradiation time for MO solution under simulated solar of 0.4 Sun is twice of that under the solar of 1 Sun. However, the difference of η caused by the different shapes of concave MLAs becomes larger under irradiation with lower intensity. Among all concave MLAs, the one using sample 11 as the template achieves the most enhancement of η of MO. Concave MLAs obtained from the masterpieces made of PHDODA perform better than those made of PLMA in accelerating the photodegradation of MO.

The variance of η obtained from different concave MLAs comes from several factors. First, concave MLAs with better transparency under irradiation contribute to a higher photodegradation rate. As shown in the transmittance spectra in Figure S6, concave MLAs made from PHDODA templates show higher transmittance under

simulated solar light, leading to more enhancement in η. Second, the uniformity of concave MLAs affects the strength of focusing effects and further influences of the photodegradation efficiency. Deformation of PLMA convex MLAs during thermal curing of PDMS leads to poorer regularity in corresponding concave MLAs, suppressing focusing effects of corresponding concave MLAs. In comparison, masterpieces made of PHDODA retain the shape and result in concave MLAs with better uniformity and performance. Last but not least, the shape of concave MLAs plays an important role in improving the η of organic pollutants. For two concave MLAs obtained from PHDODA templates, both the uniformity and transmittance are similar to each other, but the peak irradiance flux of the concave MLA with a larger aspect ratio (sample 11 as the template) is stronger according to optical simulations. As a result, more enhancement of η is observed in the reactor equipped with this concave MLA.

The photodegradation of MO assisted by PDMS concave MLAs is also conducted in river water. Similar to the degradation in ultrapure water, the concave MLA using sample 11 as the template still has better effectiveness than that made from sample 10 in enhancing MO photodegradation in river water (Figure 6E–G). Meanwhile, the photodegradation under 0.4 Sun is slower than the process under 1 Sun in river water, the same as that in ultrapure water as well. However, the η of MO in river water is generally lower than that in ultrapure water under the same irradiation conditions (Figure 6E–G). With the application of concave MLAs, the gaps of η resulting from different water matrices are narrowed. For the concave MLA presenting the highest enhancement, the difference of η when changing the water matrix after the irradiation of 45 min under 1-Sun simulated solar can even be neglected. Besides the two water matrices above, concave MLAs are also found feasible to improve η of MO in a water matrix with high turbidity (Figure S7), and the enhancement of η achieved by the concave MLA is more obvious in the solution with higher turbidity.

The effectiveness of concave MLAs in MO photodegradation is quantified by the enhancement factor defined in Equation (2) and plotted with the time of irradiation in Figure 6H,I. Based on the change of enhancement, the influence of different factors on the performance of concave MLAs is investigated. As the irradiation time becomes longer, the enhancement factor decreases due to the lower degradation rate of MO in reactors with concave MLAs in the later stage of the reaction.[23] When the intensity of irradiation decreases from 1 Sun to 0.4 Sun, the enhancement factor by concave MLAs significantly increases. In the situation of weaker irradiation (0.4 Sun), the energy barrier of the degradation of MO is hard to go over. Nevertheless, the hot spots with higher intensity are created in the top layer of the solution by using concave MLAs, making the photodegradation easier to happen under the weaker irradiation. The higher enhancement factor in river water and highly turbid water than that in ultrapure water also benefits from the redistribution of light by concave MLAs. In river water or highly turbid water, the light energy is not sufficient because of the absorbance caused by impurities or severe scattering due to particles. Concave MLAs improve the intensity in the space with focusing effects, reducing the loss of light energy and leading to higher enhancement factors.

The effect of concave MLAs on PDMS films in enhancing η is also validated with the photodegradation of another typical organic contaminant, carbendazim (CBZ), in ultrapure water. Direct photodegradation without photocatalysts and the ZnO-photocatalytic degradation process are both conducted in the presence of the concave MLA made from sample 11. According to the η obtained after the light treatment in Figure 6J,K, the concave MLA contributes to faster degradation of CBZ regardless of the existence of the photocatalyst. In the photocatalyst-assisted degradation, η significantly increases for both the control group and the concave MLA-involved group. However, the enhancement factor by the concave MLA in photocatalytic degradation is relatively smaller than that in direct photodegradation (Figure 6L), since the η in the control group with ZnO is higher due to the contribution of photocatalysts. Similar phenomenon has been observed when applying convex MLAs in photocatalytic degradation of organic contaminants.[60]

Even though the enhancement factor by the concave MLA is not outstanding, the usage of concave MLA to enhance the photodegradation of organic contaminants is still promising. On one hand, concave MLAs are able to enhance the η of different organic pollutants. On the other hand, the effectiveness of concave MLAs is proven in diverse scenarios, including different irradiation intensities, varied water matrices, and alternative degradation mechanisms (with and without photocatalysts). Furthermore, the concave MLAs can be set outside of the reactor, avoiding the adsorption of contaminants and possible photocatalyst particles, which is difficult to realize for convex MLA. Multiple concave MLAs on PDMS films can be obtained from a single convex MLA with highly tunable curvature. The thermal stability and hydrophobicity of PDMS film also make the concave MLA easy to maintain in some outdoor applications.[61–63]

3 | CONCLUSION

Aiming to mitigate the risk of detachment of microlenses and secondary contamination, non-contact concave

MLAs have been developed for enhanced photodegradation of organic pollutants in water. Convex MLA templates are fabricated with a scalable method based on multiple solvent exchange processes and local photopolymerization processes. The as-prepared concave MLAs have tunable curvatures, enabling them to be easily integrated into the solar-driven reactor for photodegradation without contact with the treated aqueous phase. The validation through confocal microscopy and optical simulations shows that the total light intensity at focal points in concave MLAs, which represents the strengths of focusing effects, is comparable with that in the convex MLAs. Additionally, the peak intensity increases by 16% in concave MLAs as the aspect ratio (depth to lateral radius) changes from 0.50 to 0.52, similar to that in convex MLA. The strong focusing effects of concave MLAs contribute a maximum enhancement by 512% and 86.3% in the photodegradation efficiency of methyl orange and carbendazim, respectively. Notably, the effectiveness of concave MLAs is also approved under irradiation with low intensity, and for real-life river water samples, or high-turbidity aqueous solutions. The non-contact mode solar-driven reactors integrated with concave MLAs can serve as a sustainable and adaptive platform for enhanced decontamination performance.

4 | EXPERIMENTAL SECTION

4.1 | Fabrication and characterization of convex MLAs templates through solvent exchange

The formation of surface microdroplet arrays are carefully controlled through a highly tunable solvent exchange process which has been previously reported.[53,57,58] In a confined 2D fluidic chamber fully filled with solution A, solution B was added to replace solution A at flow rates varying from 3 to 45 mL/h. Solution A consisted of a UV-curable monomer, photoinitiator, and a mixture of good solvent and poor solvent of monomer, while solution B was the poor solvent saturated with the monomer and photoinitiator. The UV-curable monomers used for the work included lauryl methacrylate (LMA, Acros Organics) and 1,6-hexanediol diacrylate (HDODA, 98.5%, Alfa Aesar). Surface microdroplet arrays formed due to the oversaturation induced by the solvent exchange and were pinned on the circular hydrophobic domains on pre-patterned substrates. The pre-patterned substrate was fabricated by combining the surface hydrophobization and a photolithography method reported in the literature.[56] Substrates with surface convex MLAs can be used as the new patterned substrate for more rounds of the solvent exchange process. (Figure 1A).

After the UV curing step under irradiation at the wavelength of 365 nm (Analytik Jena UV lamp) for 15 min, surface microdroplet arrays were transformed into convex MLAs. During each round of solvent exchange, the volume of microdroplets was carefully controlled by adjusting the composition of solution A or the flow rates during solvent exchange, ranging from 12 to 62 femtoliter.[53,54] The conditions for preparing MLA samples and the corresponding sample number were listed in Table 2. For sample 1–9, ethanol was the solvent in solution A, while 50 vol% ethanol aqueous solution is the solvent in solution A for sample 10 and 11. For each solution A, a photoinitiator volume equivalent to one-tenth of the monomer volume was added for subsequent photopolymerization. Planar glass substrates with two different sizes, 672 mm^2 (56 mm × 12 mm) and 100 cm^2 (10 cm × 10 cm), were applied in the fabrication of sample 1–11.

The morphology of convex MLAs was characterized by the optic microscope (Nikon H600l) equipped with a camera (Nikon DSFi3). The lateral size of a single ML and the surface coverage rate of MLA in every sample were measured and analyzed by Image J. The 3D structure of polymeric MLA was characterized by an atomic force microscope (AFM, tapping mode, Bruker Innova) and a confocal microscope (Axio CSM 700, Zeiss). The intensity profiles of polymeric MLA were acquired by capturing the light intensity around sample 1–11 through a confocal laser scanning microscope (SP8, Leica).

4.2 | Fabrication and characterization of concaveMLAs through soft lithography

To produce concave MLAs, convex MLAs, sample 8–11, were surface modified and used as templates in the soft lithography process. After cleaning and drying sample 8 and 9 at room temperature, a commercialized spray (Pro-Tex protector spray, Moneysworth & Best) was used to make the PLMA MLAs more hydrophobic at room temperature (Figure 1A). For sample 10 and 11, perfluorodecyltrichlorosilane (PFOTS, 97%, Sigma Aldrich) was coated through a chemical vapor deposition (CVD) process. During the CVD coating process, a desiccator was pre-purged by a vacuum pump (MZ1C, BrandTech) for 30 min and then placed in an oven at 100°C for 60 min. Then the cleaned and dried PHDODA MLAs were placed in the preheated desiccator with a well of 150 μL PFOTS. After purging out the air with the vacuum pump for 30 min, the desiccator was kept in the oven at 80°C for 60 min.

To imprint the structure of convex MLAs, PDMS pre-elastomer and curing agent (SYLGARD 184, Dow) was thoroughly mixed with a weight ratio of 15 to 1. The mixture was degassed within a desiccator connected to the vacuum pump for 3 h to remove the bubbles. Afterward, 20 g of the mixture was poured into a petri dish (diameter: 150 mm, PYREX), in which the functionalized polymeric surface MLA template (10 cm × 10 cm) was set at bottom center. After a curing process at 75°C for 45 min in an oven, a flexible concave MLAs-embedded crosslinked PDMS film (thickness: ~1 mm) was peeled off from the convex MLA template and then sonicated in acetone and ethanol for 10 min, respectively (Figure 1A). Surface-functionalized convex MLAs could be repeatedly used as templates for fabricating deformable concave MLAs. Similar to convex MLAs, the morphology and intensity profiles of concave MLAs were characterized by optical microscopy. Aside from AFM, the SEM (Sigma FESEM, Zeiss) was also applied to observe the top view and cross-sectional view of the PDMS concave MLA samples to get more accurate depths of each concave ML.

4.3 | Photodegradation of organic pollutants in aqueous environment with convex and concave MLA

Two typical organic contaminants, methyl orange (MO, 85%, Sigma-Aldrich) and carbendazim (CBZ, analytical standard, Sigma Aldrich), were chosen as the model compounds to compare the performance of different MLA samples in improving the photodegradation efficiency. The photodegradation was conducted in the self-assembled reactors with the length of 90 mm, the width of 80 mm, and the thickness of 1 mm (Figure 1B,C). Chemical structures of organic contaminants were shown in Figure 1D. MO aqueous solution (5 mg/L, pH = 3.0) and CBZ aqueous solution (5 mg/L, pH = 7.0) were prepared by dissolving the model compounds in ultrapure water (produced by Milli-Q Direct 16), and the pH value was adjusted by sulfuric acid solution (1 M). For the photocatalytic degradation of CBZ, 10 mg/L commercial ZnO nanoparticles (certified ACS powder, Fisher Chemical, with a band gap of 3.26 eV) were dispersed in the aqueous solution, and the solution was stored for 24 h in the dark to reach adsorption equilibrium. Simulated solar light (SS200AAA Solar Simulation Systems, Photo Emission Tech) with tunable light intensity (1 Sun = 100 mW/cm^2) was used as the light source during the photodegradation. The influence of irradiation intensity on the effectiveness of concave MLAs in photodegradation enhancement was discussed by shifting the irradiation intensity from 1 Sun to 0.4 Sun.

The effectiveness of concave PDMS MLAs was also evaluated by the photodegradation of MO in different water matrices. The water matrices used for the preparation of MO solution included ultrapure water, real river water (collected from Whitemud Creek to the North Saskatchewan River in Edmonton, Alberta, Canada on July 25, 2022), and ultrapure water dispersed with 0.2 g/L SiO_2 particles. The pH value of the MO solution prepared in all water matrices was adjusted to 3.0 with sulfuric acid solution (1 M). The original real river water had a pH value of 7.5 (Accumet AE150, Fisher Scientific), a TOC value of 25.6 mg/L (TOC-L Series, SHIMADZU), and a COD value of 163.3 mg/L (pre-dosage HANNA vials), and the SiO_2 dispersed water had a turbidity of 154.0 (±3.9) NTU (T-100 Handheld Turbidity Meter, Oakton), helping to simulate the practical wastewater.[64] MO solution with SiO_2 particles was stocked in the dark at 4°C overnight until the adsorption of MO reached the equilibrium.

The photodegradation efficiency (η) of a specific contaminant was defined in Equation (1). C_{bef} and C_{aft} were the concentration of the contaminant before and after the light treatment, respectively. According to Beer–Lambert Law, the concentration of the analyte is proportional to the absorbance value when the concentration is within a linear range. Therefore, the η of the contaminant could be A_{bef} and A_{aft} obtained with UV–visible spectroscopy (UV–vis, Thermo fisher, Genesys 150), which was the peak absorbance value of the solution before and after the light treatment, respectively. To quantify the enhancement from the surface MLAs, an enhancement factor was defined by Equation (2). In the equation, η_{MLA} was the degradation efficiency with MLA-involved treatment, and η_{ctrl} was the degradation efficiency of the contaminant in the control group, that is, the same treatment without MLA.

$$\eta = \frac{C_{bef} - C_{aft}}{C_{bef}} \times 100\% = \frac{A_{bef} - A_{aft}}{A_{bef}} \times 100\% \quad (1)$$

$$f = \frac{\eta_{MLA}}{\eta_{ctrl}} \quad (2)$$

4.4 | Optical simulations of convex and concave MLAs

Convex MLAs and concave MLAs involved in light treatment systems were modeled in three-dimensional space with Zemax OpticStudio. The light treatment system was composed of a plane wave light source (along the Z axis), a convex or concave MLA, substrates, and the aqueous phase containing organic

contaminants. Those components were organized according to the same set-up shown in Figure 1B,C. The intensity of light sources was equal to the intensity of the simulated solar light (1 Sun). For each MLA sample, an *X-Z* plane detector (6.6 μm × 80 μm) was placed along the central axis of a single ML to obtain a cross-sectional intensity profile. Horizontal light-flux (*X-Y* plane) detectors (37 μm × 37 μm) were inserted below MLAs at different *Z* positions to capture the top-view light irradiation profiles of each sample. The points with the maximum irradiation flux in all the horizontal detectors below MLAs were defined as the hot spots of MLAs. To quantify the strength of enhancing the local intensity of irradiance of all MLAs, the intensity at hot spots of MLs (I_{hs}) in each MLA sample within the area of 1 cm^2 was added up and defined as I_{Total}, and the total number of MLs within the area was *N*, as shown in Equation (3).

$$I_{Total} = \sum_{n=1}^{n=N} I_{hs} \quad (3)$$

AUTHOR CONTRIBUTIONS

Qiuyun Lu, Xuehua Zhang: Conceptualization. **Qiuyun Lu, Yanan Li, Kehinde Kassim:** Methodology, data collection, and analysis. **Qiuyun Lu, Ben Bin Xu, Xuehua Zhang:** Writing original draft, editing and review. **Mohamed Gamal El-Din, Xuehua Zhang:** Project administration and funding acquisition.

ACKNOWLEDGMENTS

The authors acknowledge the support from the Canada First Research Excellence Fund as part of the University of Alberta's Future Energy System research initiative. This research was undertaken, in part, thanks to funding from the Canada Research Chairs Program. This work was also supported by a Natural Sciences and Engineering Research Council of Canada (NSERC) Senior Industrial Research Chair (IRC) in Oil Sands Tailings Water Treatment through the support of Canada's Oil Sands Innovation Alliance (COSIA), Syncrude Canada Ltd., Suncor Energy, Inc., Canadian Natural Resources Ltd., Imperial Oil Resources, Teck Resources Limited, EPCOR Water Services, Alberta Innovates, and Alberta Environment and Parks. XHZ and MGED appreciate funding from NSERC Discovery Grant programs from NSERC Alliance-Alberta Innovates (AI) Advance grants and the support from Canada Foundation for Innovation. BBX are grateful for the support from the Engineering and Physical Sciences Research Council (EPSRC, UK) RiR grant - RIR18221018-1.

CONFLICT OF INTEREST STATEMENT

The author team wants to declare a conflict of interest that one of the author, Professor Ben B Xu, is an associate editor of EcoMat, therefore, he should be excluded from any stages in assessing this submission.

ORCID

Qiuyun Lu https://orcid.org/0000-0003-4675-9277
Ben Bin Xu https://orcid.org/0000-0002-6747-2016

REFERENCES

1. Porley V, Chatzisymeon E, Meikap BC, Ghosal S, Robertson N. Field testing of low-cost titania-based photocatalysts for enhanced solar disinfection (SODIS) in rural India. *Environ Sci*. 2020;6(3):809-816. doi:10.1039/C9EW01023H
2. Banerjee T, Podjaski F, Kroger J, Biswal BP, Lotsch BV. Polymer photocatalysts for solar-to-chemical energy conversion. *Nat Rev Mater*. 2021;6(2):168-190. doi:10.1038/s41578-020-00254-z
3. Nahim-Granados S, Rivas-Ibanez G, Pérez JAS, Oller I, Malato S, Polo-López MI. Fresh-cut wastewater reclamation: techno-economical assessment of solar driven processes at pilot plant scale. *Appl Catal B Environ*. 2020;278:119334. doi:10.1016/j.apcatb.2020.119334
4. Gong J, Li C, Wasielewski MR. Advances in solar energy conversion. *Chem Soc Rev*. 2019;48(7):1862-1864. doi:10.1039/C9CS90020A
5. Zhang P, Lou XW. Design of Heterostructured Hollow Photocatalysts for solar-to-chemical energy conversion. *Adv Mater*. 2019;31(29):1900281. doi:10.1002/adma.201900281
6. Stevens R, Miyashita T. Review of standards for microlenses and microlens arrays. *Imaging Sci J*. 2010;58(4):202-212. doi:10.1179/136821910X12651933390746
7. Fang C, Zheng J, Zhang Y, et al. Antireflective Paraboloidal microlens film for boosting power conversion efficiency of solar cells. *ACS Appl Mater Interfaces*. 2018;10(26):21950-21956. doi:10.1021/acsami.7b19743
8. Liu Q, Liu H, Li D, Qiao W, Chen G, Ågren H. Microlens array enhanced upconversion luminescence at low excitation irradiance. *Nanoscale*. 2019;11(29):14070-14078. doi:10.1039/C9NR03105G
9. Dongare PD, Alabastri A, Neumann O, Nordlander P, Halas NJ. Solar thermal desalination as a nonlinear optical process. *Proc Natl Acad Sci*. 2019;116(27):13182-13187. doi:10.1073/pnas.1905311116
10. Gao H, Hyun JK, Lee MH, Yang J-C, Lauhon LJ, Odom TW. Broadband Plasmonic microlenses based on patches of Nanoholes. *Nano Lett*. 2010;10(10):4111-4116. doi:10.1021/nl1022892
11. Dyett B, Zhang Q, Xu Q, Wang X, Zhang X. Extraordinary focusing effect of surface Nanolenses in Total internal reflection mode. *ACS Central Sci*. 2018;4(11):1511-1519. doi:10.1021/acscentsci.8b00501
12. Bae S-I, Kim K, Jang K-W, Kim H-K, Jeong K-H. High contrast ultrathin light-field camera using inverted microlens arrays with metal–insulator–metal optical absorber. *Adv Opt Mater*. 2021;9(6):2001657. doi:10.1002/adom.202001657
13. Zhong Y, Yu H, Wen Y, et al. Novel optofluidic imaging system integrated with tunable microlens arrays. *ACS Appl Mater Interfaces*. 2023;15(9):11994–12004.

14. Ma Y, Li H, Chen S, et al. Skin-like electronics for perception and interaction: materials, structural designs, and applications. *Adv Intell Syst*. 2021;3(4):2000108. doi:10.1002/aisy.202000108
15. Jürgensen N, Fritz B, Mertens A, et al. A single-step hot embossing process for integration of microlens arrays in biodegradable substrates for improved light extraction of light-emitting devices. *Adv Mater Technol*. 2021;6(2):1900933. doi:10.1002/admt.201900933
16. Vinayaka AC, Ngo TA, Nguyen T, Bang DD, Wolff A. Pathogen concentration combined solid-phase PCR on supercritical angle fluorescence microlens Array for multiplexed detection of invasive NontyphoidalSalmonellaSerovars. *Anal Chem*. 2020;92(3):2706-2713. doi:10.1021/acs.analchem.9b04863
17. Kang B-H, Jang K-W, Yu E-S, et al. Ultrafast plasmonic nucleic acid amplification and real-time quantification for decentralized molecular Diagnostics. *ACS Nano*. 2023;17(7):6507–6518.
18. Wei Y, Yang Q, Bian H, et al. Fabrication of high integrated microlens arrays on a glass substrate for 3D micro-optical systems. *Appl Surf Sci*. 2018;457:1202-1207. doi:10.1016/j.apsusc.2018.06.267
19. Cai S, Sun Y, Chu H, Yang W, Yu H, Liu L. Microlenses arrays: fabrication, materials, and applications. *Microsc Res Tech*. 2021;84(11):2784-2806. doi:10.1002/jemt.23818
20. Lee M, Lee GJ, Jang HJ, et al. An amphibious artificial vision system with a panoramic visual field. *Nat Electron*. 2022;5(7):452-459. doi:10.1038/s41928-022-00789-9
21. Sohn I-B, Choi H-K, Noh Y-C, Kim J, Ahsan MS. Laser assisted fabrication of micro-lens array and characterization of their beam shaping property. *Appl Surf Sci*. 2019;479:375-385. doi:10.1016/j.apsusc.2019.02.083
22. Ding Y, Lin Y, Zhao L, et al. High-throughput and controllable fabrication of soft screen protectors with microlens arrays for light enhancement of OLED displays. *Adv Mater Technol*. 2020;5(10):2000382. doi:10.1002/admt.202000382
23. Lu Q, Xu Q, Meng J, et al. Surface microlenses for much more efficient Photodegradation in water treatment. *ACS ES&T Water*. 2022;2(4):644-657. doi:10.1021/acsestwater.2c00008
24. Li Y, Lu Q, EI-Din MG, Zhang X. Immobilization of photocatalytic ZnO nanocaps on planar and curved surfaces for the photodegradation of organic contaminants in water. *ACS ES&T Water*. 2023;3(8):2740–2752.
25. Hanun JN, Hassan F, Jiang J-J. Occurrence, fate, and sorption behavior of contaminants of emerging concern to microplastics: influence of the weathering/aging process. *J Environ Chem Eng*. 2021;9(5):106290. doi:10.1016/j.jece.2021.106290
26. Mukaida M, Yan J. Ductile machining of single-crystal silicon for microlens arrays by ultraprecision diamond turning using a slow tool servo. *Int J Mach Tools Manuf*. 2017;115:2-14. doi:10.1016/j.ijmachtools.2016.11.004
27. Liu X, Zhou T, Zhang L, et al. 3D fabrication of spherical microlens arrays on concave and convex silica surfaces. *Microsyst Technol*. 2019;25(1):361-370. doi:10.1007/s00542-018-3971-6
28. Mo J, Chang X, Renqing D, Zhang J, Liao L, Luo S. Design, fabrication, and performance evaluation of a concave lens array on an aspheric curved surface. *Opt Express*. 2022;30(18):33241. doi:10.1364/OE.471055
29. Zhang D, Xu Q, Fang C, et al. Fabrication of a microlens Array with controlled curvature by thermally curving photosensitive gel film beneath microholes. *ACS Appl Mater Interfaces*. 2017;9(19):16604-16609. doi:10.1021/acsami.7b00766
30. Zhang Q, Guo Z, Ma Z, Wang S, Peng B. Fabricating SU-8pPhotoresist microstructures with controlled convexity--concavity and curvature through thermally manipulating capillary action in poly (dimethylsiloxane) microholes. *Langmuir*. 2023;39(2):763–770.
31. Gissibl T, Thiele S, Herkommer A, Giessen H. Two-photon direct laser writing of ultracompact multi-lens objectives. *Nat Photonics*. 2016;10(8):554-560. doi:10.1038/nphoton.2016.121
32. Li R, Li C, Yan M, et al. Fabrication of chalcogenide microlens arrays by femtosecond laser writing and precision molding. *Ceram Int*. 2023;49(10):15865–15873. doi:10.1016/j.ceramint.2023.01.181
33. Wu M, Jiang L, Li X, et al. Microheater-integrated microlens array for robust rapid fog removal. *ACS Appl Mater Interfaces*. 2023;15(34):41092–41100.
34. Chen F, Liu H, Yang Q, et al. Maskless fabrication of concave microlens arrays on silica glasses by a femtosecond-laser-enhanced local wet etching method. *Opt Express*. 2010;18(19):20334-20343. doi:10.1364/OE.18.020334
35. Deng Z, Yang Q, Chen F, et al. Fabrication of large-area concave microlens array on silicon by femtosecond laser micromachining. *Opt Lett*. 2015;40(9):1928-1931. doi:10.1364/OL.40.001928
36. Wu P, Cao X, Chen Z, et al. Fabrication of cylindrical microlens by femtosecond laser-assisted hydrofluoric acid wet etching of fused silica. *Adv Photonics Res*. 2023;4(4):2200227. doi:10.1002/adpr.202200227
37. Zhang A, Bai H, Li L. Breath figure: a nature-inspired preparation method for ordered porous films. *Chem Rev*. 2015;115(18):9801-9868. doi:10.1021/acs.chemrev.5b00069
38. Han JW, Joo CW, Lee J, et al. Enhancement of spectral stability and outcoupling efficiency in organic light-emitting diodes with breath figure patterned microlens array films. *Opt Mater*. 2019;96:109262. doi:10.1016/j.optmat.2019.109262
39. Mei L, Qu C, Xu Z, et al. Facile fabrication of microlens array on encapsulation layer for enhancing angular color uniformity of color-mixed light-emitting diodes. *Opt Laser Technol*. 2021;142:107227. doi:10.1016/j.optlastec.2021.107227
40. Kessel A, Frydendahl C, Indukuri SRKC, Mazurski N, Arora P, Levy U. Soft lithography for manufacturing scalable perovskite Metasurfaces with enhanced emission and absorption. *Adv Opt Mater*. 2020;8(23):2001627. doi:10.1002/adom.202001627
41. Li J-W, Li Y-J, Hu X-S, et al. Biosafety of a 3D-printed intraocular lens made of a poly(acrylamide-co-sodium acrylate) hydrogel in vitro and in vivo. *Int J Ophthalmol*. 2020;13(10):1521-1530. doi:10.18240/ijo.2020.10.03
42. Luan S, Xu P, Zhang Y, Xue L, Song Y, Gui C. Flexible Superhydrophobic microlens arrays for humid outdoor environment applications. *ACS Appl Mater Interfaces*. 2022;14(47):53433-53441. doi:10.1021/acsami.2c17128
43. Li T, Xu Z, Xu BB, et al. Advancing pressure sensors performance through a flexible MXene embedded interlocking structure in a microlens array. *Nano Res*. 2023;16(7):1–7.
44. Moore S, Gomez J, Lek D, You BH, Kim N, Song I-H. Experimental study of polymer microlens fabrication using partial-filling hot embossing technique. *Microelectron Eng*. 2016;162:57-62. doi:10.1016/j.mee.2016.05.009

45. Chang C-Y, Chu J-H. Innovative design of reel-to-reel hot embossing system for production of plastic microlens array films. *Int J Adv Manuf Technol*. 2017;89(5-8):2411-2420. doi:10.1007/s00170-016-9277-x
46. Yang S-P, Kim J-B, Seo Y-H, Jeong K-H. Rotational offset microlens arrays for highly efficient structured pattern projection. *Adv Opt Mater*. 2020;8(16):2000395. doi:10.1002/adom.202000395
47. Bae S-I, Kim K, Yang S, Jang K-w, Jeong K-H. Multifocal microlens arrays using multilayer photolithography. *Opt Express*. 2020;28(7):9082-9088. doi:10.1364/OE.388921
48. Peng Y, Guo X, Liang R, et al. Fabrication of microlens arrays with controlled curvature by micromolding water condensing based porous films for deep ultraviolet LEDs. *ACS Photonics*. 2017;4(10):2479-2485. doi:10.1021/acsphotonics.7b00692
49. Long Y, Song Z, Pan M, et al. Fabrication of uniform-aperture multi-focus microlens array by curving microfluid in the microholes with inclined walls. *Opt Express*. 2021;29(8):12763-12771. doi:10.1364/OE.425333
50. Liu X-Q, Yu L, Yang S-N, et al. Optical nanofabrication of concave microlens arrays. *Laser Photonics Rev*. 2019;13(5):1800272. doi:10.1002/lpor.201800272
51. Zhang X, Ren J, Yang H, He Y, Tan J, Qiao GG. From transient nanodroplets to permanent nanolenses. *Soft Matter*. 2012;8(16):4314. doi:10.1039/c2sm07267j
52. Yu H, Peng S, Lei L, Zhang J, Greaves TL, Zhang X. Large scale flow-mediated formation and potential applications of surface Nanodroplets. *ACS Appl Mater Interfaces*. 2016;8(34):22679-22687. doi:10.1021/acsami.6b07200
53. Zhang X, Lu Z, Tan H, et al. Formation of surface nanodroplets under controlled flow conditions. *Proc Natl Acad Sci*. 2015;112(30):9253-9257. doi:10.1073/pnas.1506071112
54. Lu Z, Peng S, Zhang X. Influence of solution composition on the formation of surface Nanodroplets by solvent exchange. *Langmuir*. 2016;32(7):1700-1706. doi:10.1021/acs.langmuir.5b04630
55. Martí Jerez E, Fernández Pradas JM, Serra P, Duocastella M. Substrate reshaping for optically tuned liquid-printed microlenses beyond their wetting properties. *Adv Mater Technol*. 2023;8(19):2300564. doi:10.1002/admt.202300564
56. Bao L, Rezk AR, Yeo LY, Zhang X. Highly ordered arrays of Femtoliter surface droplets. *Small*. 2015;11(37):4850-4855. doi:10.1002/smll.201501105
57. Lei L, Li J, Yu H, Bao L, Peng S, Zhang X. Formation, growth and applications of femtoliter droplets on a microlens. *Phys Chem Chem Phys*. 2018;20(6):4226-4237. doi:10.1039/C7CP06861A
58. Bao L, Pinchasik B-E, Lei L, et al. Control of Femtoliter liquid on a microlens: a way to flexible dual-microlens arrays. *ACS Appl Mater Interfaces*. 2019;11(30):27386-27393. doi:10.1021/acsami.9b06390
59. Murai Y, Yoshikawa M. Polymeric pseudo-liquid membranes from poly(dodecyl methacrylate): KCl transport and optical resolution. *Polym J*. 2013;45(10):1058-1063. doi:10.1038/pj.2013.30
60. Lu Q, Yang L, Chelme-Ayala P, Li Y, Zhang X, El-Din MG. Enhanced photocatalytic degradation of organic contaminants in water by highly tunable surface microlenses. *Chem Eng J*. 2023;463:142345. doi:10.1016/j.cej.2023.142345
61. Liu Z, Sun B, Shi T, Tang Z, Liao G. Enhanced photovoltaic performance and stability of carbon counter electrode based perovskite solar cells encapsulated by PDMS. *J Mater Chem A*. 2016;4(27):10700-10709. doi:10.1039/C6TA02851A
62. Liu X, Cheng K, Cui P, et al. Hybrid energy harvester with bifunctional nano-wrinkled anti-reflective PDMS film for enhancing energies conversion from sunlight and raindrops. *Nano Energy*. 2019;66:104188. doi:10.1016/j.nanoen.2019.104188
63. Kang J, Huang R, Guo S, et al. Suppression of ion migration through cross-linked PDMS doping to enhance the operational stability of perovskite solar cells. *Sol Energy*. 2021;217:105-112. doi:10.1016/j.solener.2021.01.025
64. Lapointe M, Barbeau B. Characterization of ballasted flocs in water treatment using microscopy. *Water Res*. 2016;90:119-127. doi:10.1016/j.watres.2015.12.018

SUPPORTING INFORMATION

Additional supporting information can be found online in the Supporting Information section at the end of this article.

How to cite this article: Lu Q, Li Y, Kassim K, Xu BB, Gamal El-Din M, Zhang X. Concave microlens arrays with tunable curvature for enhanced photodegradation of organic pollutants in water: A non-contact approach. *EcoMat*. 2024;6(1):e12426. doi:10.1002/eom2.12426